An Integrated Liquid Mixer/Valve

Joel Voldman, *Student Member, IEEE*, Martha L. Gray, *Member, IEEE*, and Martin A. Schmidt, *Member, IEEE*

***Abstract*—We present an integrated liquid mixer/valve to be used for sample preparation for bioscience analysis systems. The mixer/valve is a glass-silicon bonded structure with a wafer-bonded cantilever-plate flapper valve and deep reactive-ion etched ports. It is passively pressure actuated and is distinguished by the fact that it can perform both a mixing and valving function simultaneously to mix two liquids noncontinuously. We present the design and fabrication of the mixer/valve and show that it successfully performs both its valving and mixing functions, including the discontinuous mixing of two liquids. We propose a method for characterizing mixing in this device using fluorescence microscopy and the pH dependence of fluorescein fluorescence. This method aims to allow one to extract the mixing length from a quantifiable observable. We present modeling and results of mixing length measurements using this method. [516]**

***Index Terms*—Fluid flow, fluorescense, liquid valving, microfluidics, micromachining, mixers, wafer bonding.**

I. Introduction

In RECENT years, microfabrication has been increasingly coupled to biology and medicine to produce useful devices. One area of interest is in systems for chemical, biochemical, biological, and biomedical analysis. Such systems have the potential to decrease the cost, increase the accuracy, and decrease the labor involved in performing assays as compared to macroscale systems.

Most of the work in this field has been concerned with sample analysis as opposed to sample preparation. It is clear, however, that in order for microfabricated analysis systems to reach their full potential, they must be coupled to microfabricated sample preparation systems. This paper concerns the development and characterization of a microfabricated sample preparation system consisting of a device that acts as both mixer and valve, allowing for the noncontinuous mixing of two liquids. The device would be used as a front end for a microfabricated analysis system where both mixing and valving of liquids is necessary.

Many types of microfabricated mixers and valves have already been realized. In the area of mixing alone, several different approaches have been used. At the microscale, where liquid mixing is dominated by diffusion, mixers work by creating flow patterns in which the diffusion lengths (and, hence, times) are small. One micromixer [1] used a plate with holes to break one liquid stream into narrow jets, thus shortening the diffusive mixing time. References [2] and [3] repeatedly separated and rejoined the fluid streams, layering them each time and thus cutting the diffusion time needed for mixing. Recently, [4] used laminar chaotic advection, which mixes two liquids by constructing a flow field whereby small differences in a fluid particle's initial location lead to large differences in its final location. This causes a chaotic rearrangement of the fluid particles, thus mixing the two liquids. These designs differ from this paper because they are continuous-mixing devices, which do not incorporate valving function, whereas this paper allows for the discrete mixing of two liquids using its integrated valve.

The type of valve used with the liquid mixer/valve is a cantilever-plate flapper valve. One of the first cantilever-plate flapper valves over an anisotropically etched cavity was fabricated by Tirén *et al.* in 1989 [5]. In 1990, Ohnstein *et al.* fabricated an electrically actuated flapper valve for gas handling [6]. Emmer *et al.* used cantilever-plate flapper valves for chromatography [7]. More recently, flapper valves have been used as parts of pumps [8]. Finally, two groups have performed coupled hydro-mechanical simulations of cantilever-plate flapper valves to evaluate their performance [9]–[11].

II. Device Structure and Specifications

The structure of the integrated liquid mixer/valve is shown in Fig. 1(a), while relevant dimensions of the cantilever plate area are shown in Fig. 1(b). The liquid mixer/valve consists of a lower silicon wafer with a cantilever-plate flapper valve and fluid ports. This wafer is anodically bonded to an upper glass wafer that contains the fluidic channel. The left-hand side of Fig. 1(a) reveals an enlargement of the reagent-inlet port area. The cantilever-plate flapper valve is shown atop the reagent inlet port and valve seat.

To derive specifications for the mixer/valve, we used flow cytometry as a model analysis system. Flow cytometry was chosen because it uses whole cells, has several simplified preparation protocols [12], and has been shown to be amenable to microfabrication [13]. A total sample volume of 1 μL was chosen as the minimum sample size necessary to contain a statistically significant number of white blood cells. The time needed to prepare the total sample volume should be approximately 30 s, while the mixing time should be approximately 2 s. This mixing time is not particularly aggressive, but does not need to be for this application. The mixer/valve should be able to handle a variety of mixing ratios (sample to reagent volume ratios), from all sample to all reagent. In order to ensure that cells can flow through the device, all dimensions in the cell flow-path must be larger than 40 μm. Finally, the device must be a low-pressure device, operating with less than 10 lbf/in^2 of pressure.

Manuscript received December 23, 1999; revised April 20, 2000. Subject Editor, O. Tabata.

J. Voldman and M. A. Schmidt are with the Department of Electrical Engineering and Computer Science and the Microsystems Technology Laboratories, Massachusetts Institute of Technology, Cambridge, MA 02139 USA.

M. L. Gray is with the Department of Electrical Engineering and Computer Science, the Microsystems Technology Laboratories, and the Department of Health Sciences and Technology, Massachusetts Institute of Technology, Cambridge, MA 02139 USA.

Publisher Item Identifier S 1057-7157(00)08026-4.

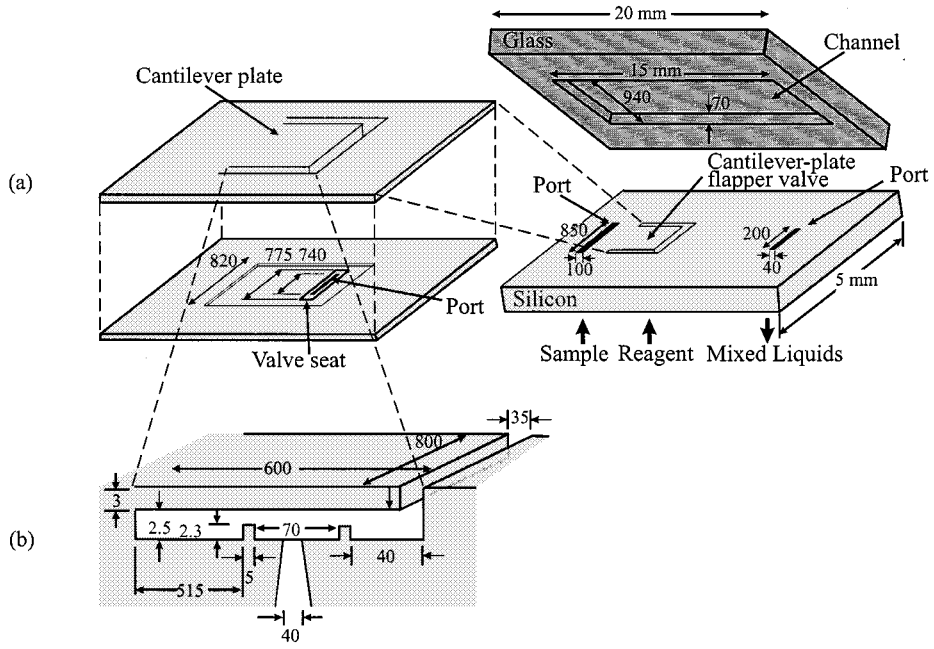

Fig. 1. Schematic of the integrated liquid mixer/valve. (a) Overall bonded structure showing the silicon wafer with a cantilever-plate flapper valve and ports, and the glass wafer with flow channels. (b) Relevant dimensions of the cantilever plate area. (Not to scale. Unless noted otherwise, all dimensions are in micrometers.)

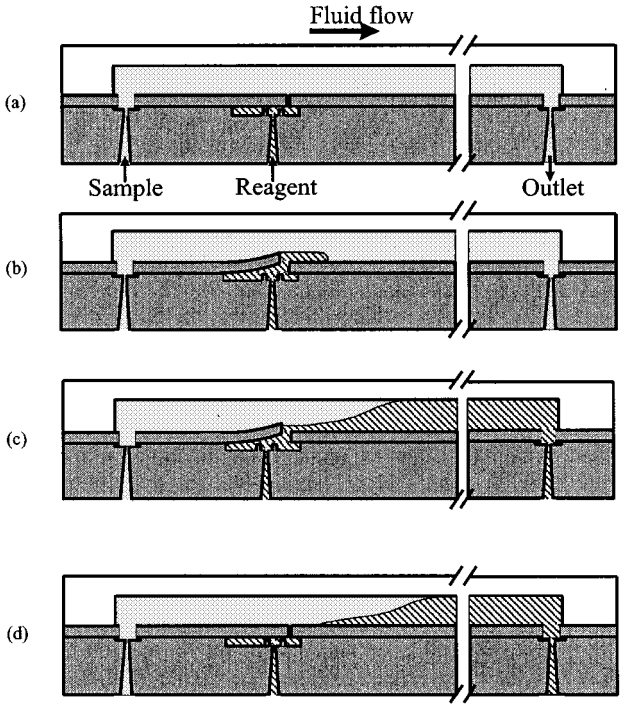

Fig. 2. Operation of liquid mixer/valve.

III. Operation

The schematic operation of the liquid mixer/valve is shown in Fig. 2. At time zero, sample flows down the channel [see Fig. 2(a)]. When it is time to mix a reagent with the sample, the reagent is injected into the sample stream [see Fig. 2(b)], and the two mix diffusively in a few seconds [see Fig. 2(c)]. After the desired section of sample is prepared, the reagent is shut off [see Fig. 2(d)] and the mixed sample and reagent flow down the channel and out of the liquid mixer/valve.

The liquid mixer/valve is controlled by varying the reagent and sample flow rates. The relative flow rates (and whether they are actually flowing), in turn, determine the mixing ratio and pressures at the reagent and sample ports; the cantilever plate aligns itself accordingly. Thus, the device is passively pressure actuated.

IV. Design and Simulation

A first-order design was undertaken to establish the overall chip dimensions and dimensions of the fluidic channel. The first-order design decouples the interaction between the hydraulics of the fluidic channel and the mechanics of the plate, thus allowing quick design turnaround. The hydraulics consist of the two inlet channels connected together with the outlet channel. Continuity relationships are used with the total volume and run-time specifications to determine the appropriate channel geometries.

Numerical simulations were then undertaken to determine the flapper valve and valve seat geometries. The first simulation determines the pressure-flow relationship for the cantilever-plate flapper valve in a quasi-one-dimensional (1-D) manner. The algorithm works by first assuming a plate deflection for a given flow rate. From this initial deflection, the pressure distribution under the plate is calculated using lumped pressure elements, as in [9]. The simulation accounts for flow out the side of the plate through the use of parallel and perpendicular lumped fluidic resistances. The calculated pressure distribution is then fed into a finite-difference beam code, which calculates the linearized beam deflection from

$$EI\frac{\partial^4 w}{\partial x^4} = q(x) \tag{1}$$

where $w(x)$ is the deflection of the beam, E and I are its biaxial modulus and moment of inertia, respectively, and $q(x)$ is the

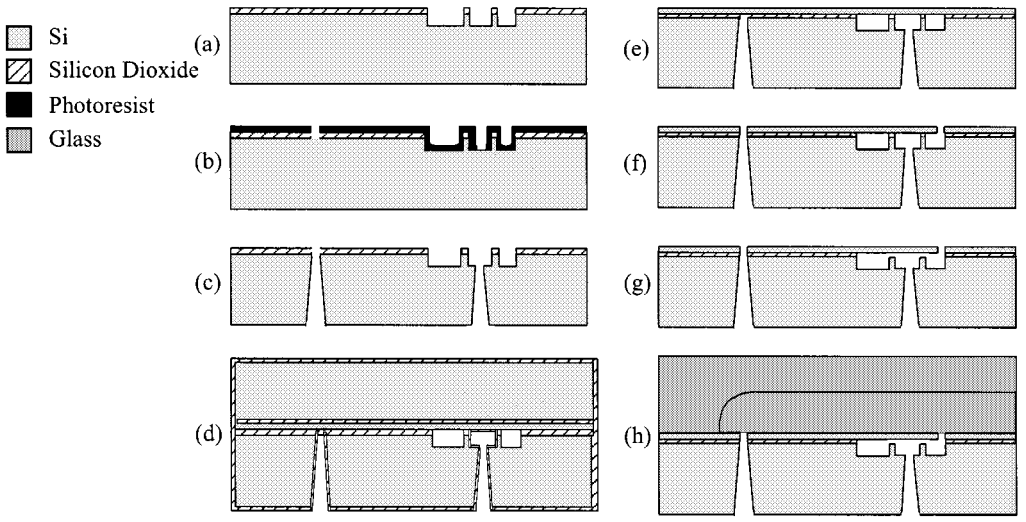

Fig. 3. Fabrication process flow for the mixer/valve.

distributed pressure load. This beam deflection is then used to calculate a new pressure distribution, and so on until the two solutions converge.

A second algorithm computes the sample flow rate necessary to close the valve. This algorithm uses the channel geometry and flapper valve geometry to compute lumped fluidic resistances that are then used with the beam bending equation (1) to determine the minimum flow rate necessary to cause the cantilever plate to bend down and contact the valve seat. While only an estimate of the necessary closing flow rate, it is a useful design marker.

In order to assure that the mixing times will be within specifications, the 1-D time-dependent diffusion equation was analytically solved for the boundary conditions of no flow through the walls and different initial ratios of sample and reagent (mixing ratio). Since the mixing time is dependent on the square of the channel height, this lets us choose the channel height to minimize mixing time while still being large enough for cells to flow through.

The final geometries are shown in Fig. 1(b).

V. Fabrication

A. Silicon Fabrication

The process flow for fabricating the liquid mixer/valve is shown in Fig. 3. The process starts with 100-cm double-side-polished wafers. First, 2000 Å of thermal oxide is grown [see Fig. 3(a)]. This layer has two functions. It: 1) defines the distance between the top of the valve seat and the bottom of the cantilever plate and 2) keeps the plate fastened to the valve seat throughout the fabrication process, enhancing its robustness. After the oxide is grown, a photolithography step, a buffered oxide etch (BOE), and a plasma etch define the valve seat itself.

Following this the fluidic ports are patterned using thick photoresist (AZ4620, Hoechst AG, Strasbourg, France) and the ports are etched using a deep reactive-ion-etching (deep-RIE) system [see Fig. 3(b) and (c)]. An important requirement for this etch is that the reagent port hole be located within the valve seat, which requires optimizing the exposure/develop/etch process to allow etching of a hole (the port) in a depression next to another feature (the valve seat).

Following the port etch, the wafers are cleaned and fusion bonded to SOI wafers (3-μm silicon overlayer, 0.2 μm of buried oxide). The wafers are annealed at 1100 °C in an oxidizing ambient to grow a 1-μm protective oxide [see Fig. 3(d)]. The oxide is then stripped from the top side of the bonded pair with HF vapor and the bulk silicon is removed from the device wafer with potassium hydroxide (20% w/w, 60 °C). Following this the buried oxide is stripped in BOE [see Fig. 3(e)]. The flapper plate is then defined and plasma etched [see Fig. 3(f)]. The final step consists of a buffered oxide etch to release the cantilever plate from the valve seat [see Fig. 3(g)]. When the plate is free, the wafers are dried using a three-step water/methanol/isopropanol process to minimize stiction between the plate and the valve seat.

Fig. 4 shows three views of the completed device. Fig. 4(a) shows the cantilever plate area with the cantilever plate removed. The port hole etch and valve seat can be seen. The other ridges in the valve seat area are strength bars used to hold and strengthen the cantilever plate during processing. Fig. 4(b) shows a close-up of the top of the reagent port hole, showing the surface roughening that occurs near the top of the deep-RIE etch [14]. Fig. 4(c) shows the freed cantilever plate.

B. Glass Etching

The glass etching process is a conglomeration of processes developed by various other researchers (see, e.g., [15]). The 100-cm glass wafers (Corning 7740, Mooney Precision Glass, Huntington, WV) are first subjected to a three-part clean consisting of a 15-min detergent clean (Alconox, Alconox Inc., White Plains, NY), a 10-min Piranha clean (3:1 H_2SO_4:H_2O_2), and a 45-min UV-ozone clean. The glass wafers are then immediately inserted into an electron-beam evaporation system, where 200 Å of chrome and 2000 Å of gold are deposited. Next, the wafers are coated with photoresist and the channels are patterned in the photoresist. The gold is then etched in aqua regia (3:1 HCl:HNO_3), and the chrome is etched with a commercial chrome etchant (CR-7). This leaves a tri-layer masking

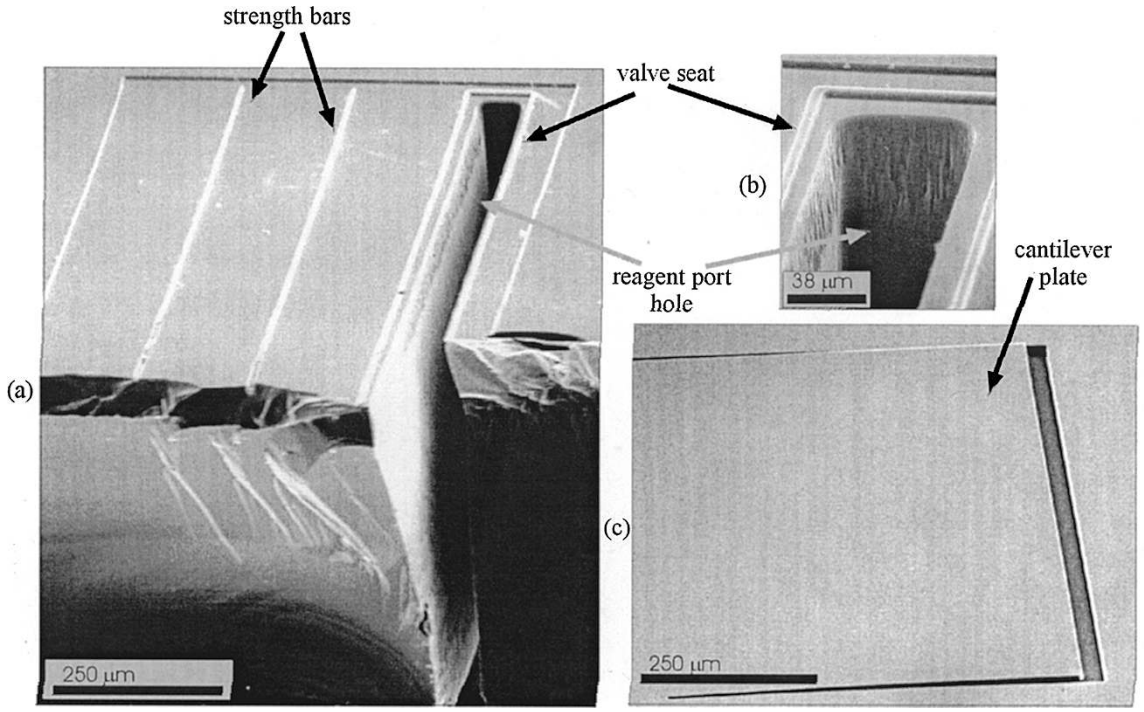

Fig. 4. Electron micrographs of completed structure. (a)–(b) Valve seat area with plate removed. (c) Final structure with released plate.

system. The Cr/Au layer is the main mask for the glass etching, while the photoresist helps to protect the glass against pinholes in the Cr/Au layers. The glass is etched in a solution of 66:14:20 water:HNO_3:HF until the desired etch depth is obtained. With this process, the anisotropy ratio is about 1.2–1.3, which is close to an ideal isotropic etch, indicating that the mask is not being severely undercut by the etchant.

C. Anodic Bonding

The final step is to align and anodically bond the glass and silicon wafers. The alignment is performed on a special jig in a commercial aligner and the anodic bonding is performed on a hot plate setup with the following parameters: temp = 350 °C–400 °C, weight ∼ 10 lb, voltage = 800 V.

VI. Packaging

The liquid mixer/valve chips are packaged, as shown in Fig. 5(a). First, the wafer is diced into chips, and then each chip is glued into a machined aluminum block that contains holes for the three fluidic ports. Screws with holes drilled through the middle are butted up against o-rings that press against the chip, creating an internal seal. Tubing (0.51 mm I.D. TYGON, Norton Performance Plastics, Wayne, NJ) is glued to the screws to provide the fluid. With this setup, the liquid only wets the tubing, screw, o-ring, and chip. The assembly has been tested for leakage using carbon dioxide as the fluid and can hold pressure up to at least 10 lbf/in^2, which is sufficient for these experiments.

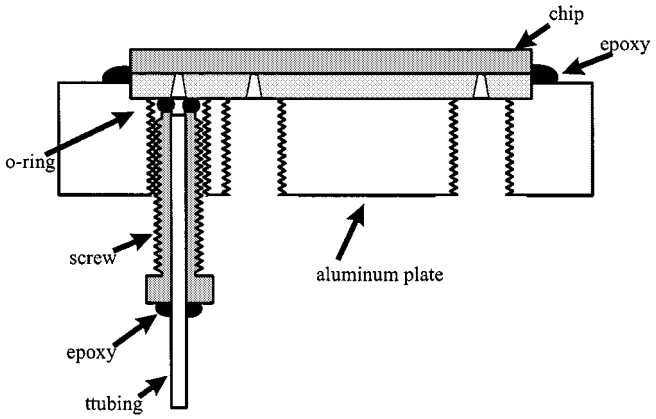

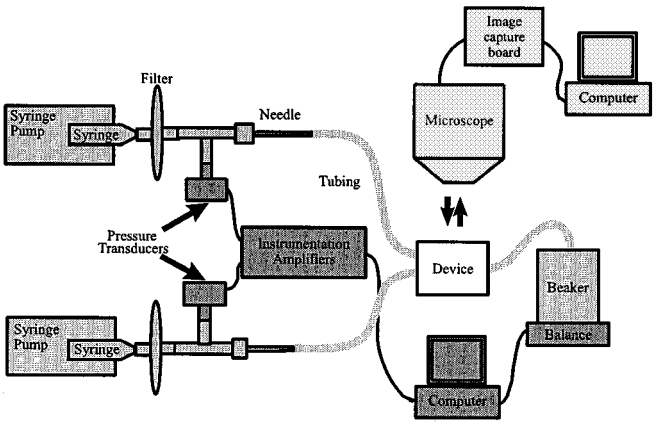

Fig. 5. (a) Packaging setup for mixer/valve chip. For clarity, the screw with tubing is not shown for the other two ports. (b) Setup used for testing the devices.

VII. Test Setup

The test setup [see Fig. 5(b)] consists of the following three sections:

1) fluidics to apply and control the flows;
2) electronics to monitor and record pressures and flow rates in the system;
3) microscope to record images and fluorescence from the chip.

Using this system, we monitor the following variables—both inlet pressures, inlet flow rates, and outlet flow rate, and fluorescence intensity along the channel.

The fluidics consist of two syringe pumps and luer-locked components, which provide constant flow rates. The syringe pumps (KD Scientific, New Hope, PA, and Orion Research Inc., Beverly, MA) drive syringes (1 mL, Hamilton, Reno, NV), which are connected to syringe filters (1-μm pore size, Micron Separations Inc., Westborough, MA), and then connected to tubing via syringe needles (25s gauge, Hamilton, Reno, NV), and finally to the chip.

The electrical system uses two pressure transducers (Honeywell Microswitch, Freeport, IL) connected to the flow system to monitor the upstream inlet pressures. The output from the pressure transducers are fed into instrumentation amplifiers and then connected to the computer-control system. The flow rates are monitored via either the syringe pumps or a mass-flow system. The complete electronics are controlled with a computer running Labview (National Instruments, Austin, TX).

The optics consist of a Zeiss Axiovert inverted microscope (Carl Zeiss Inc., Thornwood, NY) with a silicon-intensified-target camera (Hamamatsu C2400, Hamamatsu Corporation, Bridgewater, NJ). The camera output is fed into an image acquisition system and processed with a commercial package (Image-1, Universal Imaging Corporation, West Chester, PA).

VIII. Valving Function

One of the two functions of the integrated mixer/valve is a valving function. The liquid mixer/valve should allow sample to flow down the channel while preventing reagent from flowing when not wanted, and then open and allow mixing when the pressure differentials are adjusted accordingly.

To test leakage of sample into reagent, fluid was flown into the sample inlet port, down the channel, and out the outlet port. The reagent port was left open to atmosphere. The flow rates into the device and out of the device were measured. Agreement between the two flow rates would indicate that no fluid was going out the reagent port; the cantilever-plate flapper valve is closing correctly. Any deviation would indicate leakage into the reagent port. The device was tested under a range of flow rates (0–30 μl/min), causing pressure differentials of up to 310 Pa. No leakage was detected to within experimental error.

Leakage of reagent into the sample stream was tested visually—at zero sample flow rate, the reagent leaked from the reagent port into the channel via diffusion, as expected. As the sample flow was increased the cantilever plate is expected to bend down and seal the reagent port. Consistent with this prediction, we observed that fluorescence leakage from the reagent port disappeared.

Upon application of flow to the reagent port, the flapper valve opened as expected. It exhibited mostly linear pressure-flow characteristics because the channel sections upstream and downstream from the cantilever plate (and their linear flow resistances) were the dominant resistances. A problem encountered with measuring pressure-flow relationships of the mixer/valve (and also for general operation) is that the small gap between the valve seat and cantilever plate causes the device to be very prone to clogging. Once debris is lodged between the valve seat and flap, the valving function is no longer functional; filtration of reagents is critical to the proper operation of the mixer/valve. This problem is not crucial for flow cytometry applications because cells would be considered the sample and would, hence, be flowed through the inlet port. All dimensions in the cells' path would then be at least 70 μm.

IX. Mixing Length

The second important function of the liquid mixer/valve is its use as a mixer. Measuring the mixing length first requires a definition of mixing length. For this paper, we chose the mixing length as the length fluid must flow, after which there is less than 5% variation in analyte concentration across the cross section of the flow.

The difficulty with measuring the mixing length for this device is that the lamination of flow is in the z-axis. As we have no way of looking sideways at the chip to see the two fluid streams, we must develop a method that looks from the top down.

One way to measure the mixing length would be to use a fluorescent dye coupled with a confocal microscopy system. This would allow the researcher to reconstruct the three-dimensional flow profile and to, hence, determine where along the channel the dye concentration stops changing. Confocal-scanning microscopy, while giving all the necessary information, also gives more information than needed (the full three-dimensional profile). In addition, reconstructing the flow profile from the cross sections is slow and cumbersome.

In pursuit of a single measurement for mixing-length determination, we have adapted work done on measuring mixing in turbulent flows [16]–[18]. This method uses the fact that the fluorescence quantum yield of the fluorescent dye fluorescein is pH dependent. In a basic medium ($\mathrm{pH} > 10$), the fluorescence quantum yield of fluorescein approaches 1.0—the fluorescence is on. In acidic media ($\mathrm{pH} < 3$), the fluorescence quantum yield of fluorescein approaches $\sim$0.3—the fluorescence is off.

With these two facts, the following experiment can be envisioned. If fluorescein in a basic solution is mixed with an acidic solution, such that the final solution is acidic, then the fluorescein will go from being ON to being OFF (Fig. 6). Locating the point where this transition occurs will locate the point where the pH is approximately neutral. The length from the onset of mixing to this point is dubbed the fluorescence turn-off length (FTOL). If a model is formed that can correlate the FTOL with a simulated mixing length, then we can infer the mixing length for an arbitrary species of known diffusivity by measuring the FTOL.

The experimental protocol was as follows: 1-mM solutions of HCl and 0.1-mM solutions of NaOH where made. A water-sol-

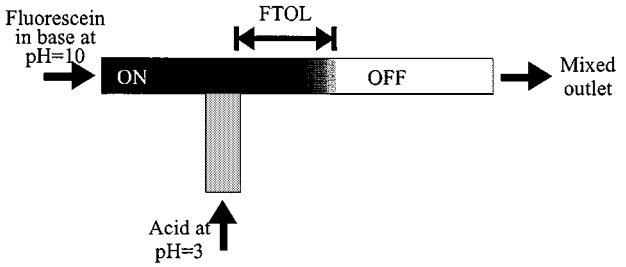

Fig. 6. Definition of the FTOL. A basic solution of fluorescein is mixed with an acid, such that the final pH is acidic. The fluorescence will go from being ON to turning OFF. The distance this takes is the FTOL.

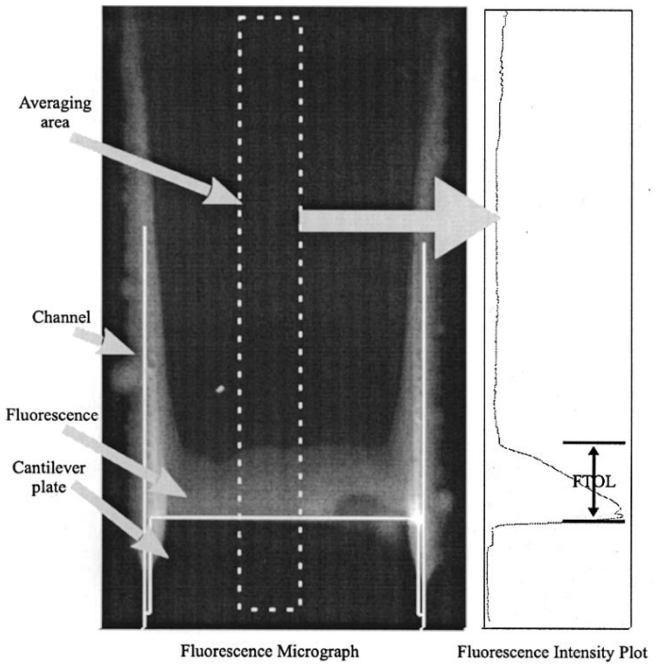

Fig. 7. Overview of the experimental method, showing how the FTOL data is extracted from the fluorescence micrographs. The fluorescence intensity from a swath of the image is extracted, averaged, and the FTOL is calculated from the resulting intensity values. For this micrograph, the sample flow rate was 10 μm/min and the reagent flow rate was 20 μm/min.

uble salt of fluorescein (Aldrich Chemical Corporation, Milwaukee, WI) was added to the NaOH solution to make a 10-μM fluorescein solution. The acid was used as the sample, and the fluorescein+base was used as the reagent. Various flow rates and mixing ratios were run and the pictures of the valve area were taken (Fig. 7). The images were corrected for illumination nonuniformity.

As can be seen from Fig. 7, the fluorescence intensity is nonuniform near the edges of the channel. This is due to increased flow of the reagent from the side of the plate coupled with decreased flow of sample near the walls, increasing the fluorescence turn-off length in this area. To simplify our analysis, we avoid this inherently three-dimensional problem by performing our mixing length computations on areas near the center of the channel, where our 1-D model is appropriate.

The pixel intensities across a small swath of valve were extracted via image analysis software and these were averaged to create an intensity profile plot. The FTOL from each profile was then extracted with software routines. These images

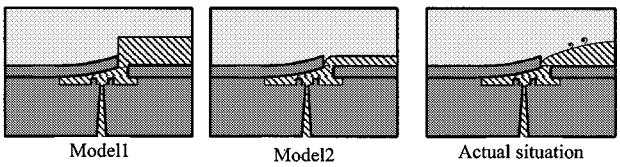

Fig. 8. Different diffusion models for calculating the FTOL. The first model (left) computes the initial reagent height from the mixing ratio, while the second model (middle) uses the pressure differential-induced plate deflection to calculate the initial reagent height. The actual situation (right) will be a conglomeration of the two.

clearly show the reagent entering the channel through the valve and mixing with the sample flowing over the cantilever plate (Fig. 7). Remaining fluorescence nonuniformities in the center of the channel are likely due to microparticles disturbing the flow from under the cantilever plate.

It is necessary to point out and to emphasize that the FTOL is NOT the same as the mixing length. The FTOL is a measure of the pH of the solution. The pH is not linearly related to the proton concentration—rather, it is the negative logarithm of the proton concentration. In addition, the diffusivities of the acid, base, and fluorescein are different and, thus, the acid/base will not mix in the same amount of time as the fluorescein.

In order to match the data with a model, simulations from two slightly different models were run using Matlab. The simulations modeled three-component time-dependent diffusion with reaction using a Crank–Nicholson implicit scheme. The simulations start with the initial concentration profiles for the hydrogen ions (H^+), hydroxyl groups (OH^-), and fluorescein. The hydrogen ions and hydroxyl groups are allowed to diffuse for one time step. Then the two species are reacted, and the new concentration profiles calculated. This process is continued until sufficient time has elapsed. From the concentration profiles of the H^+ and OH^-, the pH of the solutions can be calculated for all time. Finally, the fluorescence quantum yield of fluorescein is calculated from the pH using data from the literature [19].

Next, the fluorescein concentration for all time is calculated using an analytical formula as described above in the design section. The fluorescein concentration is integrated along the height of the channel along with its fluorescence quantum yield to give the simulated intensity profile. The fluorescence turn-off points are extracted from the simulated intensity profiles in an identical manner to the measured profiles.

The first diffusion model (Fig. 8, left-hand side) calculates the initial sample and reagent heights in the channel from the mixing ratio, and uses an overall average flow velocity to compute the distance traveled versus time. The second model (Fig. 8, middle) uses the plate deflection derived from the simulated pressure-flow relationship to predict the sample and reagent heights in the channel, and calculates the reagent flow rate from the geometry of the valve opening. Both of these models approximate the flow rate as being uniform along the cross section of the channel.

These two models can be seen as extremes of the physical situation. The first model overstates the initial reagent height since the cantilever plate does not displace past 10 μm at the flow rates of interest. The second model underestimates the initial reagent height since the reagent does not exit the flap only moving along

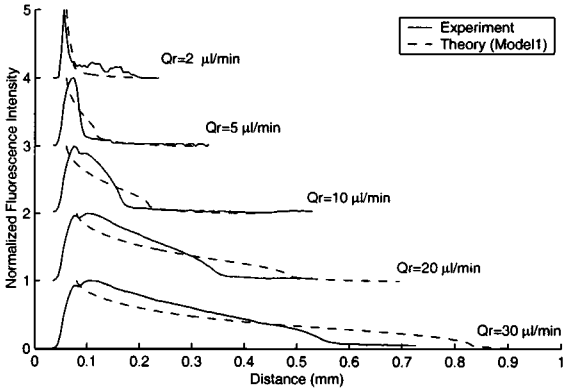

Fig. 9. Comparison of experimental and simulated fluorescence intensity profiles for a sample flow rate of 5 μm/min. Each fluorescence intensity profile has been normalized to one fluorescence intensity unit and displaced along the fluorescence intensity axis.

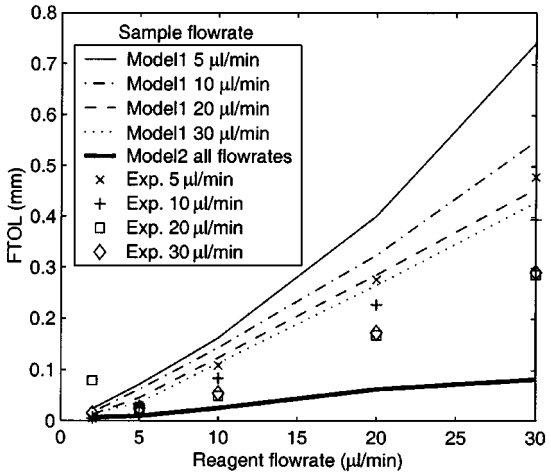

Fig. 10. Comparison of measured and simulated FTOL for different sample and reagent flow rates.

the channel. The first model also underestimates the flow rate in the channel, while the second model overestimates it, neglecting that mixing between the two streams will lower the reagent flow rate. The actual situation would be a meld of the two models (Fig. 8, right-hand side).

Experimentally derived and simulated fluorescence intensity profiles (for the first diffusion model) for one sample flow rate are shown in Fig. 9. The corresponding FTOLs are shown in Fig. 10, while some measured FTOLs are given in Table I. Also shown in Table I are parameters extracted from the simulations. The fluorescence turn-off times listed are computed from the fluorescence-intensity versus time simulations. Assuming that the FTOL model is valid, as evidenced by the agreement between the experimental and predicted FTOLs (Fig. 10), the mixing times and lengths can then be extracted from the analytical fluorescein diffusion simulations (Table I). Mixing lengths are derived from the mixing times by incorporating the flow velocity calculated using the first diffusion model.

The trends in the simulated results using each model can be quantitatively explained by noting that the FTOL will be the product of the velocity used by each model with the fluorescence turn-off time, which increases with initial increasing

TABLE I
QUANTITIES MEASURED AND EXTRACTED FROM SIMULATIONS. SHOWN ARE THE MEASURED FTOL, COMPUTED FLUORESCENCE TURN-OFF TIME (USING MODEL 1), AND SIMULATED MIXING LENGTH AND TIMES FOR FLUORESCEIN (BASED UPON ANALYTICAL DIFFUSION MODEL)

Sample (μL/min)	5	5	30	30
Reagent (μL/min)	5	30	5	30
	Measured quantity			
FTOL (mm)	0.02	0.48	0.02	0.29
	Calculated quantities			
Fluorescence turn-off time (s)	0.008	0.05	0.001	0.02
Mixing Length (mm)	9.4	18.6	36.3	55.5
Mixing Time (s)	3.7	2.1	4.1	3.7

reagent height because the amount of base needing to be neutralized increases. In the context of the first model (Fig. 8, left-hand side), as the reagent flow rate increases for a constant sample flow, the average velocity in the channel will increase. In addition, the initial height of reagent in the channel will increase because it is determined by the ratio of the sample and reagent flow rates. Both of these factors work to increase the FTOL as the reagent flow rate increases. For a given reagent flow rate, however, as we increase the sample flow rate the FTOL decreases. This is because the fluorescence turn-off time decreases due to the decreased initial reagent height in the channel outweigh the increased average flow rate, causing a net FTOL decrease.

For the second model (Fig. 8, middle), the initial reagent height in the channel is determined by the cantilever plate deflection, which is overwhelmingly controlled by the reagent flow rate, varying little as the sample flow rate changes. As the reagent flow rate increases for a constant sample flow rate, the reagent velocity will increase and, because the flap deflection increases, the overall FTOL will increase. As the sample flow rate varies for a given reagent flow rate, neither the reagent velocity nor the initial reagent height vary, causing no changes in the FTOL.

As can be seen, the FTOLs for the data lie in-between the two extreme simulations, lending validity to the simulations. Since the trends in the data mimic the first model more closely than the second, the first model may be closer to the physical situation than the second model. The fact hat the simulations model diffusion-based mixing and bound the data is consistent with diffusion being the predominant mixing mechanism. Extracting mixing times and lengths from the simulations, we see that they are within specifications. (These results also emphasize that the fluorescence-turn off point is not the same as the mixing length. If one calculates times based on the measured FTOLs (Table I) one would conclude that the two liquids would be mixing within milliseconds, which is plainly incorrect.)

X. CONCLUSION

We have presented the design and fabrication of an integrated liquid mixer/valve. The integrated liquid mixer/valve successfully performs both valving and mixing functions simultaneously and, as we have shown, allows for the noncontinuous mixing of two liquids. We have started developing a

new methodology for testing the mixing performance of this and other liquid mixers. The data and simulations presented suggest that the mixing times for the liquid mixer are similar to those expected by diffusion and within our specifications.

ACKNOWLEDGMENT

The authors wish to thank the Microsystems Technology Laboratories, Massachusetts Institute of Technology, Cambridge, and their staff for help with fabrication, and the Shriners Burns Institute (especially W. Holmes), Boston, MA, for assistance and resources during testing. The authors also wish to thank U. D. Larsen, Microelektronik Centret, Lyngby, Denmark, for his help with packaging, especially the internal seal.

REFERENCES

[1] R. Miyake, T. S. J. Lammerink, M. Elwenspoek, and J. H. J. Fluitman, "Micro mixer with fast diffusion," in *7th Int. Conf. Solid-State Sens. Actuators*, 1993, pp. 248–253.

[2] N. Schwesinger, T. Frank, and H. Wurmus, "A modular microfluid system with an integrated micromixer," *J. Micromech. Microeng.*, vol. 6, pp. 99–102, 1996.

[3] J. Branebjerg, P. Gravesen, J. P. Krog, and C. R. Nielsen, "Fast mixing by lamination," in *Proc. IEEE Microelectromech. Syst. Workshop Dig.*, 1996, pp. 441–446.

[4] J. Evans, D. Liepmann, and A. P. Pisano, "Planar laminar mixer," in *Proc. IEEE Microelectromech. Syst. Workshop Dig.*, 1997, pp. 96–101.

[5] J. Tirén, L. Tenerz, and G. Hök, "A batch-fabricated nonreverse valve with cantilever beam manufactured by micromachining of silicon," *Sens. Actuators*, vol. 18, pp. 389–396, 1989.

[6] T. Ohnstein, T. Fukiura, J. Ridley, and U. Bonne, "Micromachined silicon microvalve," in *Proc. IEEE Microelectromech. Syst. Workshop Dig.*, 1990, pp. 95–98.

[7] A. Emmer, M. Jansson, J. Roeraade, U. Lindberg, and B. Hök, "Fabrication and characterization of a silicon microvalve," in *J. Microcolumn Separations*, vol. 4, 1992, pp. 13–15.

[8] R. Zengerle, S. Kluge, M. Richter, and A. Richter, "A bidirectional silicon micropump," in *Proc. IEEE Microelectromech. Syst. Workshop Dig.*, 1995, pp. 19–24.

[9] J. Ulrich, H. Füller, and R. Zengerle, "Static and dynamic flow simulations of a KOH-etched micro valve," in *8th Int. Solid-State Sens. Actuators Conf.*, 1995, pp. 17–20.

[10] M. Koch, A. G. R. Evans, and A. Brunnschweiler, "Coupled FEM simulation for the characterization of the fluid flow within a micromachined cantilever valve," *J. Micromech. Microeng.*, vol. 6, pp. 112–114, 1996.

[11] J. Ulrich and R. Zengerle, "Static and dynamic flow simulation of a KOH-etched microvalve using the finite-element method," *Sens. Actuators A, Phys.*, vol. 53, pp. 379–385, 1996.

[12] L. W. M. M. Terstappen, H. Meiners, and M. R. Loken, "A rapid sample preparation technique for flow cytometric analysis of immunofluorescence allowing absolute enumeration of cell subpopulations," *J. Immunolog. Methods*, vol. 123, pp. 103–112, 1989.

[13] D. Sobek, S. D. Senturia, and M. L. Gray, "Microfabricated fused silica flow chambers for flow cytometry," in *Proc. IEEE Solid-State Sens. Actuator Workshop Dig.*, 1994, pp. 260–263.

[14] A. A. Ayón, C. C. Lin, R. Braff, R. Bayt, H. H. Sawin, and M. Schmidt, "Characterization of a time multiplexed inductively coupled plasma etcher," *J. Electrochem. Soc.*, vol. 146, no. 1, pp. 339–349, 1999.

[15] Z. Fan and D. J. Harrison, "Micromachining of capillary electrophoresis injectors and separators on glass chips and evaluation of flow at capillary intersections," *Anal. Chem.*, vol. 66, pp. 177–184, 1994.

[16] M. M. Koochesfahani and P. E. Dimotakis, "Mixing and chemical reactions in a turbulent liquid mixing layer," *J. Fluid Mech.*, vol. 170, pp. 83–112, 1986.

[17] D. A. Walker, "A fluorescence technique for measurement of concentration in mixing liquids," *J. Phys. E, Sci. Instrum.*, vol. 20, pp. 217–224, 1987.

[18] J. A. Bellerose and C. B. Rogers, "Measuring mixing and local pH through laser induced fluorescence," *Laser Anemometry—1994, Advances Applicat.*, vol. FED-191, pp. 217–220, 1994.

[19] M. M. Martin and L. Lindqvist, "The pH dependence of fluorescein fluorescence," *J. Lumin.*, vol. 10, pp. 381–390, 1975.

Joel Voldman (S'92) received the B.S. degree in electrical engineering from the University of Massachusetts at Amherst, in 1995, the M.S. degree in electrical engineering from the Massachusetts Institute of Technology (MIT), Cambridge, in 1997, and is currently working toward the Ph.D. degree in electrical engineering at MIT. His Ph.D. research concerns the development of single-cell traps using dielectrophoresis.

Mr. Voldman is a former National Science Foundation Graduate Research Fellow and a current Kodak Graduate Research Fellow.

Martha L. Gray (S'78–M'85), photograph and biography not available at time of publication.

Martin A. Schmidt (S'88–M'88) received the B.S. degree in electrical and computer engineering from Rensselaer Polytechnic Institute, Troy, NY, in 1981, and the S.M. and Ph.D. degrees in electrical engineering and computer science from the Massachusetts Institute of Technology (MIT), Cambridge, in 1983 and 1988, respectively. His Ph.D. research concerned microsensors for measurement of turbulent boundary layers.

In 1988, he joined the faculty of the Electrical Engineering and Computer Science Department, MIT, where he is currently a Professor of electrical engineering. He is also the Director of the Microsystems Technology Laboratories, MIT. His research interests are in microfabrication technologies for realization of micromechanical and biological reactors, micromachined turbine engines, and microactuators. He has served on the program committees for many of the major meetings in the microelectromechanical systems (MEMS) field and currently serves on the International Steering Committee for Solid-State Sensors and Actuators.

Dr. Schmidt was the recipient of the National Science Foundation Presidential Young Investigator Award and the Ruth and Joel Spira Teaching Award presented by MIT.